Article

Deformation Behavior and Microstructure Evolution of a TiB-Reinforced Ti-6.5Al-2Zr-1Mo-1V Matrix Composite

Maxim Ozerov [1], Nikita Stepanov [1,*], Vitaly Sokolovsky [1], Ilya Astakhov [1], Margarita Klimova [1], Alexander Galtsev [1], Lujun Huang [2] and Sergey Zherebtsov [1]

[1] Laboratory of Bulk Nanostructured Materials, Belgorod State University, 308015 Belgorod, Russia; ozerov@bsu.edu.ru (M.O.); sokolovskiy@bsu.edu.ru (V.S.); astakhov@bsu.edu.ru (I.A.); klimova_mv@bsu.edu.ru (M.K.); galtsev@bsu.edu.ru (A.G.); zherebtsov@bsu.edu.ru (S.Z.)
[2] College of Materials, Harbin Institute of Technology, Harbin 150001, China; huanglujun@hit.edu.cn
* Correspondence: stepanov@bsu.edu.ru

Abstract: A Ti-6.5Al-2Zr-1Mo-1V/TiB metal-matrix composite with 10.0 vol.% of TiB reinforcing fibers was produced using vacuum arc melting and compared with an unreinforced arc-melted Ti-6.5Al-2Zr-1Mo-1V alloy. The initial microstructure of the composite consisted of two-phase α + β matrix with randomly distributed boride fibers. The addition of TiB fibers resulted in a 40% increase in strength. At room temperature, the composite attained a yield strength of 1100 MPa and a ductility of 10% in compression. At elevated temperatures (400–950 °C), the values of yield strength of the composite remained ~1.5–2 times greater in comparison with the unreinforced alloy. A faster development of globularization in the composite in comparison with the unreinforced alloy was established. The interphase TiB particle/matrix boundary did not contain either a transition layer or any defects like pores or microcracks. Using the obtained results, the apparent activation energy of the plastic deformation was calculated, and processing maps were analyzed both for the unreinforced alloy and for the composite.

Keywords: titanium alloy; metal-matrix composite; microstructure; mechanical properties; globularization

1. Introduction

Titanium alloys deservedly won the leading place in aerospace and shipbuilding industries due to their high specific strength, processability, and high corrosion resistance [1,2]. Titanium alloys can also be used in parts operating at elevated temperatures, for example, in aircraft turbine compressors; however, a noticeable decrease in strength due to the lack of high-temperature strengthening mechanisms can limit their utilization at 550–600 °C. Specifically, a near-alpha Ti-6.5Al-2Zr-1Mo-1V alloy is used for manufacturing hull structures operating up to 500 °C [3]. An increase in heat resistance of this alloy is an important task, since it can significantly expand the scope of its application and replace heavier steels and nickel alloys [1–4].

The main strengthening mechanism at elevated temperatures in near-alpha titanium alloys is solid solution strengthening. The efficiency of this mechanism can be varied via modification of their chemical composition; however, this approach is well studied, and its use has diminished. Strengthening heat or thermomechanical treatments are not quite effective for the near-alpha alloys; however, this approach can be used for parts operating below 400–500 °C. Another promising way to improve strength at room and elevated temperatures can be associated with the introduction of refractory ceramic phases into a titanium matrix and thus the creation of metal-matrix composites (MMCs) [5,6]. One of the candidates of such ceramic reinforcements is TiB particles that are well matched with the titanium matrix (with both the alpha- and beta-phases), without the formation of a transition region. Furthermore, a thermal expansion coefficient close to titanium matrix and good thermal stability of TiB can provide efficient strengthening even at elevated

temperatures [5–7]. Due to their lower density and high specific strength, replacing heat-resistant alloys or steels with MMCs can result in up to 40% of weight reduction and that makes MMCs extremely promising materials for the aerospace, automotive, and shipbuilding industries [1,2,7]. At the same time, it should be noted that, at temperatures above 600 °C, titanium begins to interact actively with oxygen, and above 700 °C, with nitrogen [1,2]. Therefore, a long-term operation with titanium alloys at temperatures above 600 °C is limited by the relatively low oxidation resistance of the titanium matrix rather than by temperature softening. Therefore, the main efforts in improving their high-temperature properties should be focused on increasing strength their in the temperature range of up to 600 °C; however, the development of thermal barrier coatings can considerably increase the operating temperatures of titanium alloys [8,9].

Meanwhile, previous studies have shown a positive effect of strengthening boride particles on the high-temperature properties of as-cast titanium alloys with a single-phase alpha structure. In particular, numerous studies demonstrated that MMCs reinforced with various ceramic particles can be operated at temperatures 100–200 °C higher than those made with industrial heat-resistant titanium alloys, reaching an operating temperature range of 600–800 °C [10,11].

However, upon crystallization, borides usually form rather large needle-like precipitates, which can lead to a decrease in ductility and crack resistance [5–7,12], and further studies focused on the effect of deformation treatment on mechanical properties are needed. The results obtained earlier clearly indicate that the properties of metal-matrix composites are largely determined by the morphology of the reinforcing particles and their distribution in the matrix [5,6]. Specifically, many studies have shown that thermomechanical treatment can modify the structure of the matrix and reinforcing components, thereby improving the strength/ductility balance of composites [5,6,11,12]. Some increase in ductility is associated with the breaking of brittle components into smaller fragments during the thermomechanical treatment [7,12,13]. Moreover, a decrease in the value of the aspect ratio coefficient k (the length-to-diameter ratio of the reinforcing elements generally increases the flow stress of the composite, and, accordingly, leads to an increase in characteristics related to strength: fatigue, hardness, wear, etc.) [5,7,12]. At the same time, the probability of brittle fracture and propagation of a crack from a particle to the matrix increases with an increase in the length of the reinforcements [7,10]; this obviously leads to a decrease in ductility and crack resistance. The morphology of TiB fibers (and, as a consequence, strength and ductility of the composite) can be changed by deformation. In particular, a decrease in temperature and an increase in strain result in some decrease in the length of TiB fibers, reaching a stable value of k [12], which determine the main mechanism of strengthening (in particular, at k ≤ 10, the Orowan strengthening mechanism predominates [12]). Recent results show that well-known types of thermomechanical processing such as multiaxial isothermal forging, hot rolling, and extrusion can be used to obtain the best strength/ductility balance in MMCs [12–15].

It is worth noting that although an adequate amount of information is available on the mechanical properties of composites based on pure titanium, there are significantly fewer similar studies on composites based on near-alpha titanium alloys like Ti-6.5Al-2Zr-1Mo-1V. This study focused on the effect of boride reinforcement on the microstructure evolution and strength properties of the Ti-6.5Al-2Zr-1Mo-1V alloy at room and elevated temperatures. Mechanical properties of a TiB-reinforced Ti-6.5Al-2Zr-1Mo-1V MMC at room temperature and the effect of hot deformation at 750–950 °C on microstructure evolution and mechanical properties were studied. The obtained results can be used for selecting optimal parameters for thermomechanical processing of Ti-6.5Al-2Zr-1Mo-1V/TiB composites.

2. Materials and Methods

Laboratory-sized blanks (60 g) of the Ti-6.5Al-2Zr-1Mo-1V/TiB composite were produced using vacuum arc melting of pure (≥99.9 wt.%) Ti, Al, Zr, Mo, and V granules and

3 wt.% of CP powder of TiB_2 (99.9% purity). The unreinforced Ti-6.5Al-2Zr-1Mo-1V alloy was also fabricated using the same method without the addition of TiB_2.

The specimens measured $4 \times 4 \times 6$ mm^3 were cut using a Sodick AQ300L electro-discharge machine (Sodick Inc., Schaumburg, IL, USA). Then, specimens were isothermally compressed to obtain 50% height reduction with a mechanical testing machine Instron 300LX (INSTRON, Norwood, MA, USA) in air at 20, 400, 600, 800, 900, and 950 °C at a nominal strain rate of 10^{-3} s^{-1}. Microstructures of the initial and deformed conditions of the unreinforced alloy and composites were investigated using a FEI Quanta 600 (Thermo Fisher Scientific, Hillsboro, OR, USA) scanning electron microscope (SEM). Specimens for SEM were prepared by thorough mechanical polishing; for a clearer view of borides in the structure of the composites, deep etching (for ~5 min) was performed using the Kroll's reagent (95% H_2O, 3% HNO_3, 2% HF). Samples for TEM research were mechanically thinned to ~100 μm and then electrolytically polished at −35 °C and 29 V using an electrolyte of the following composition: 60 mL perchloric acid, 600 mL methanol, and 360 mL butanol. The resulting thin foils were studied using a transmission electron microscope (TEM) JEOL JEM 2100 (JEOL, Tokyo, Japan). The Digimizer software (version 6.3.0, MedCalc Software Ltd., Ostend, Belgium) was used to determine the average length or diameter of borides. For each condition, at least 300 measurements were taken. Phase composition of the MMC was investigated using X-ray diffraction (XRD) on an ARL-Xtra diffractometer (Thermo Fisher Scientific, Portland, OR, USA) with Cu K radiation.

Strain rate jump compressive tests were conducted at strain rates of 10^{-2}, 5×10^{-3}, 10^{-3}, and 5×10^{-4} s^{-1} in the temperature interval of 750–950 °C. Then, the activation energy of plastic deformation for the alloy and composite was calculated. To determine the optimal thermomechanical processing parameters, a processing map was constructed using the obtained results for a true strain of 0.2. To this end, power dissipation efficiency (η) was evaluated in comparison with an ideal linear dissipater (i.e., at m = 1), η = 2m/(m + 1), with the strain rate sensitivity of flow stress m = $\Delta \log \sigma / (\Delta \log \dot{\varepsilon})$ (here σ and $\dot{\varepsilon}$ are the flow stress and strain rate, respectively). The processing map is a three-dimensional projection of the area, describing η isolines depending on the strain rate and temperature on the T-$\dot{\varepsilon}$ surface [16].

3. Results

3.1. Initial Microstructures

The initial structure of the as-cast Ti-6.5Al-2Zr-1Mo-1V unreinforced alloy consisted of colonies of α-lamellae in the β-matrix. The size of α-colonies and β-grains were found to be ~100 μm and ~2 mm, respectively (Figure 1a,b). The 6.5Al-2Zr-1Mo-1V/TiB composite in the initial as-cast condition comprised of the two-phase α/β matrix with a relatively homogeneous distribution of TiB fibers spaced ~25 μm from each other (Figure 1c–f). X-ray analysis also suggested the presence of α-, β-, and TiB phases in the composite (Figure 1g). Peaks corresponding to titanium borides are typical for metal-lmatrix composites based on titanium [7,12]. The size of α-colonies (~60 μm) was comparable with the average spaces between the TiB fibers. In both materials, the volume fraction of the β phase was no more than 4%. The TiB fibers had a needle-like shape with a prismatic cross-section; the faces of TiB were created by the (100), (101), and (10$\bar{1}$) planes (Figure 1f). The average apparent length and cross-section of TiB fibers were ~26 μm and ~2.6 μm, respectively (Figure 1c,d,f). The volume fraction of TiB in the composite was found to be ~10%. The thickness of the α-lamellae was ~500 nm in the alloy and ~800 nm in the composite (Figure 1b,e). The thickness of β-interlayers was ~150 nm in both materials.
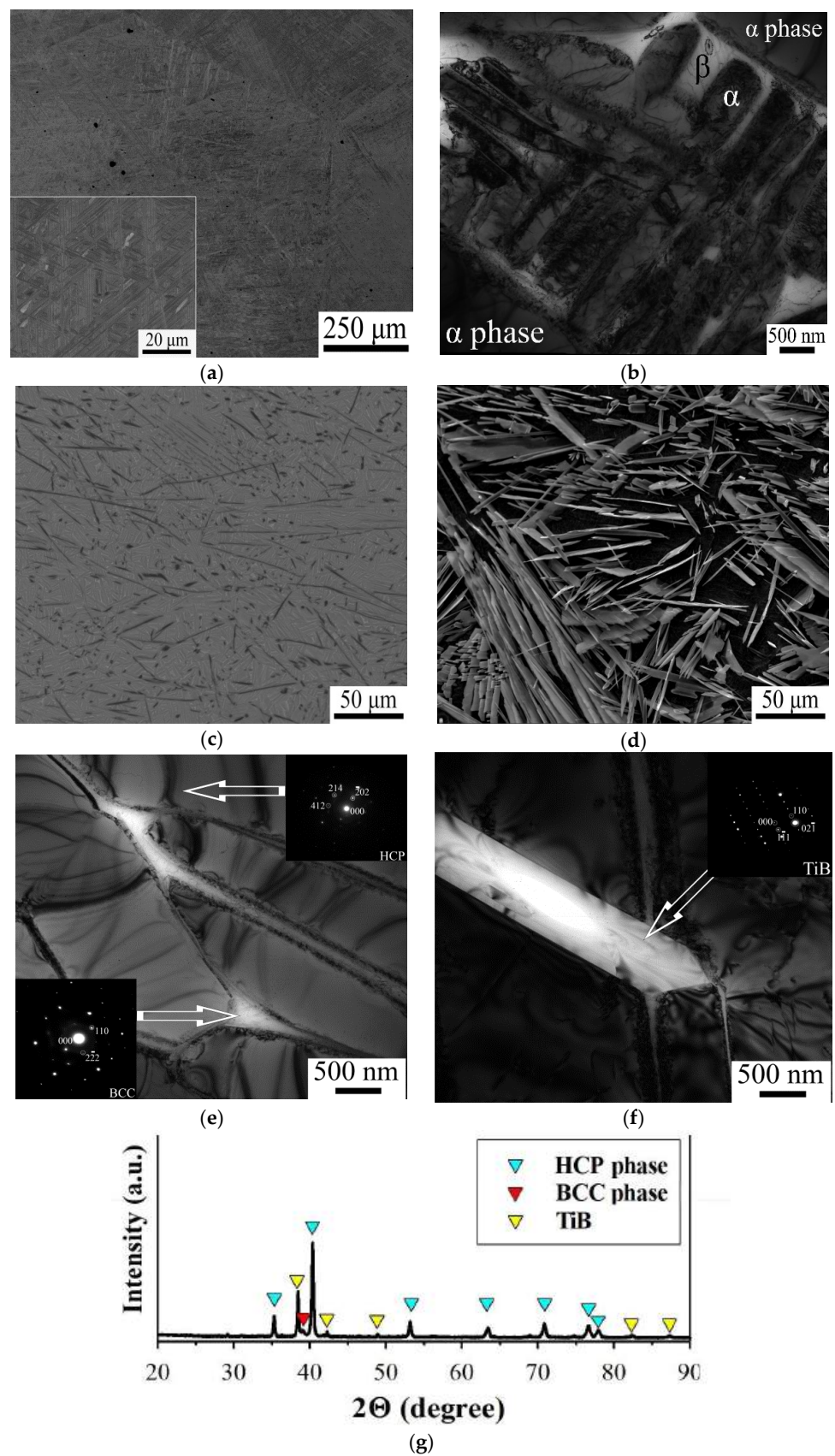
Figure 1. Initial microstructure of the Ti-6.5Al-2Zr-1Mo-1V unreinforced alloy (**a**,**b**) and Ti-6.5Al-2Zr-1Mo-1V/TiB composite (**c**–**f**); (**a**,**c**) SEM images, (**d**) SEM image of etched surface, (**b**,**e**,**f**) TEM images, and (**g**) XRD pattern of the composite.

3.2. Mechanical Behavior

The addition of 10 vol.% of TiB significantly influenced the mechanical properties of the composite in comparison with the unreinforced alloy (Figure 2, Table 1). At room temperature, the unreinforced Ti-6.5Al-2Zr-1Mo-1V alloy demonstrated a yield strength of 800 MPa and a compression ductility of 18% (Table 1, Figure 2a). The TiB fibers contributed to a 40% increase in strength (to 1100 MPa) and some decrease in ductility (Table 1, Figure 2b). Well-known studies have shown that the aspect ratio of TiB in fibers is a determining factor that influences the mechanical properties of composites [7,12]. In the initial structure of the composite, the aspect ratio was equal to ~10, and it decreased slightly (~1.2–1.5 times) after deformation, which may indicate that the Orowan mechanism is the main strengthening mechanism for this composite [12,17]. At temperatures above 400 °C for the alloy and 600 °C for the composite, their mechanical behavior changes from continuous strengthening to steady-state flow after undergoing the initial hardening transient (Figure 2). The observed softening with strain at elevated temperatures can most likely be related to recrystallization and/or dynamic globularization processes typical to warm/hot deformation of titanium alloys or titanium-based composites [12,18,19]. At 400 °C, the specimens of both materials fractured in the range of ~10–15% of height reduction; however, compression ductility was above 40% for the alloy at 600 °C, and for the composite, at 800 °C. The yield strength of the composite remained ~2 times higher till 950 °C. The higher yield strength values of the composite look quite promising (Table 1, Figure 2b) with respect to high temperature properties. These strength values turned out to be higher compared to the known values of Ti/TiB and Ti-15Mo/TiB MMCs [12,18].
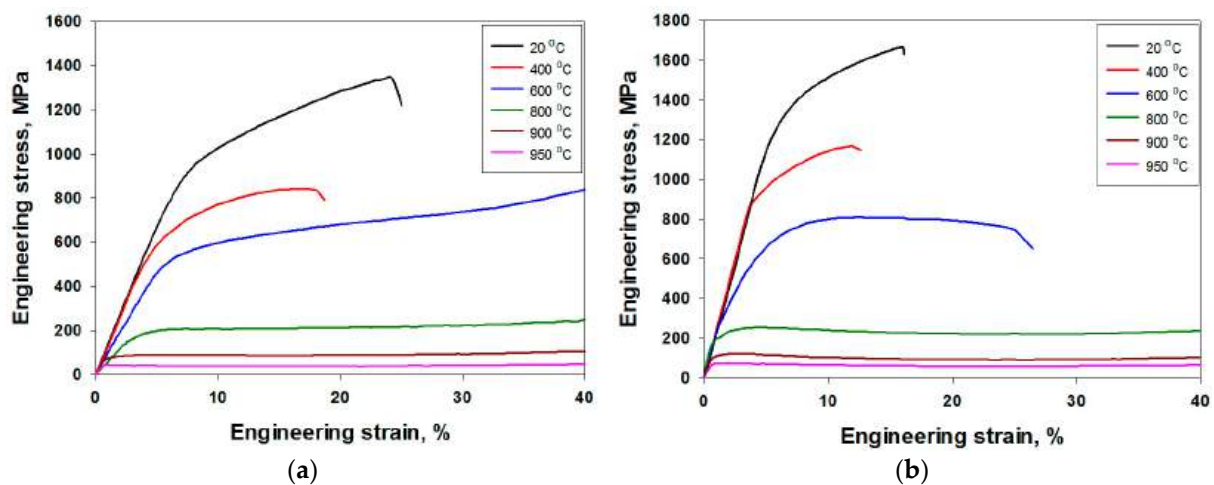

(a)   (b)

Figure 2. Flow curves obtained during compression at 20–950 °C for the Ti-6.5Al-2Zr-1Mo-1V unreinforced alloy (**a**) and Ti-6.5Al-2Zr-1Mo-1V/TiB composite (**b**).

Table 1. Compression yield strength for the unreinforced alloy and composite at various deformation temperatures.

Compression Temperature, °C	Yield Strength, MPa	
	Ti-6.5Al-2Zr-1Mo-1V Unreinforced Alloy	Ti-6.5Al-2Zr-1Mo-1V/TiB Composite
20	800	1100
400	470	750
600	440	620
800	130	250
900	60	110
950	35	70

3.3. Microstructure after Compression at 800–950 °C

It should be noted that studies on the microstructure evolution are presented starting from a deformation temperature of 800 °C, since the composite sample after compression at 600 °C collapsed without reaching a deformation degree of ~25%. The microstructure evolution of the alloy during its deformation at 800–950 °C is associated with either alignment of α-lamellae along the metal flow direction or globularization of the α-phase, depending on the initial spatial orientation (Figure 3a–c). As a result, a partially spheroidized microstructure was formed after compression. The rate of globularization increased with temperature (Figure 4a); however, this process almost did not develop at 400 and 600 °C.
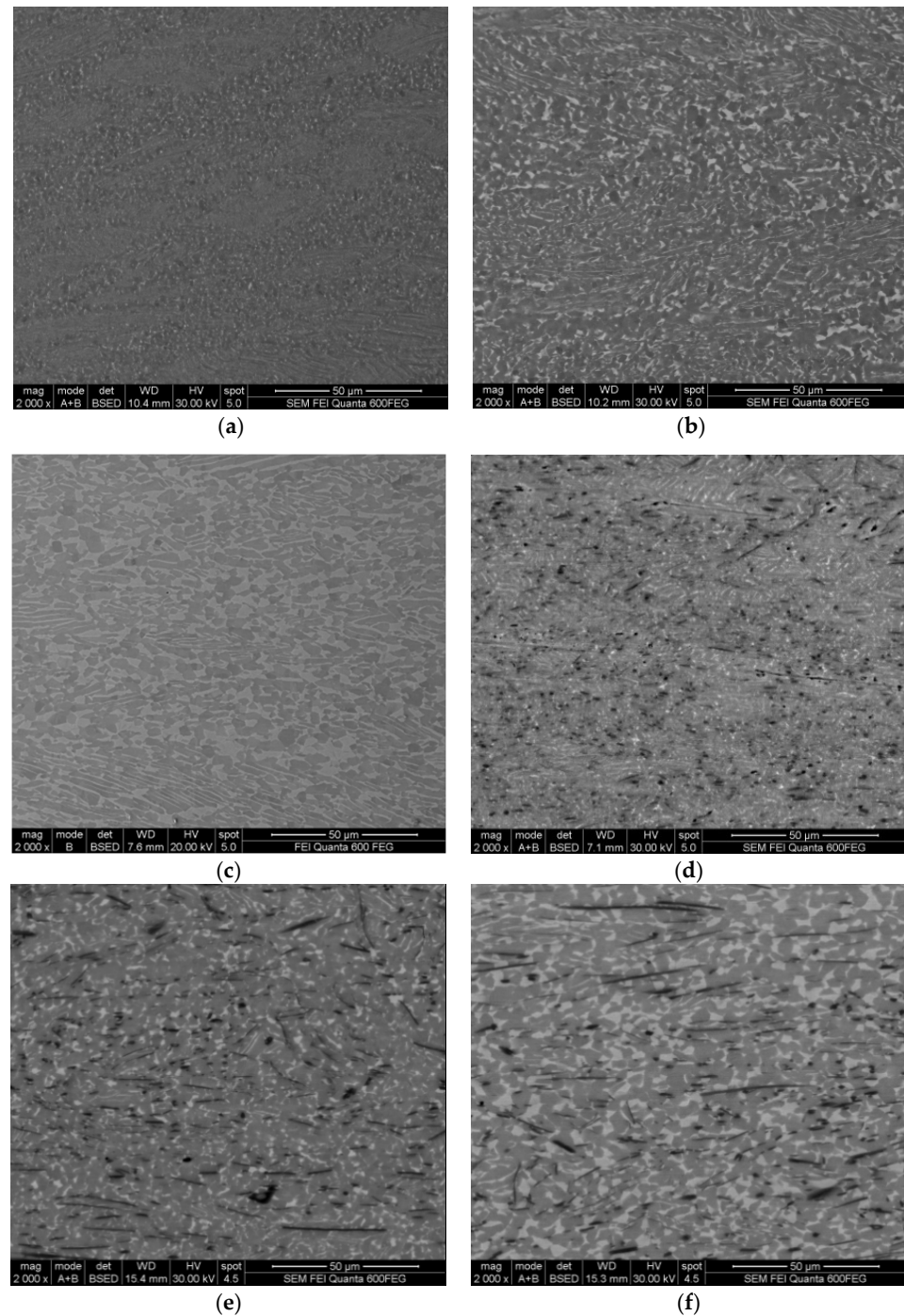
Figure 3. SEM images of the unreinforced alloy (**a–c**) and composite (**d–f**) after compression at 800 °C (**a,d**), 900 °C (**b,e**), and 950 °C (**c,f**).
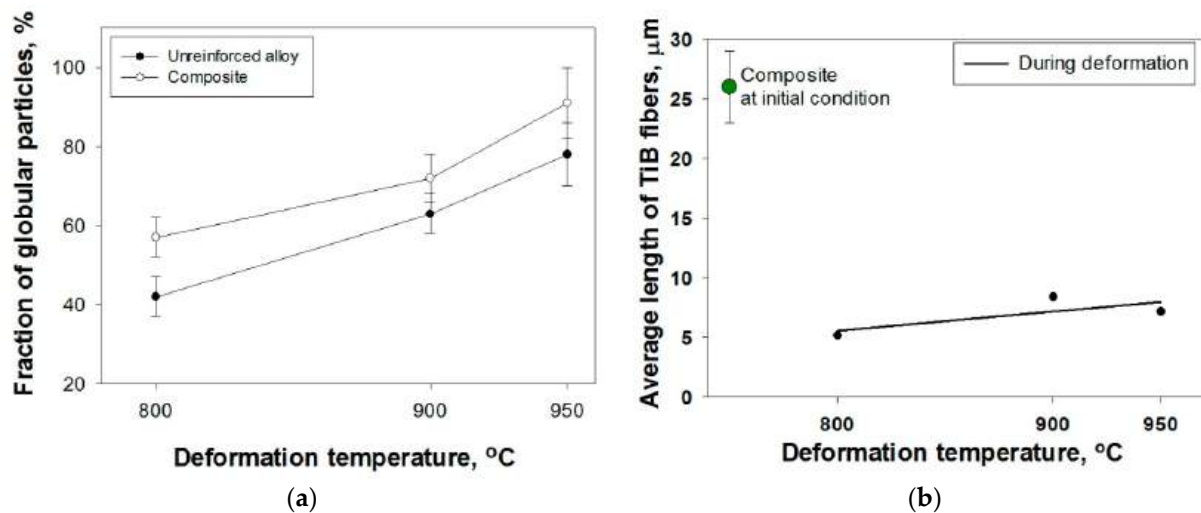
Figure 4. The fraction of globular particles during deformation at 800–950 °C (**a**) and the apparent length of the TiB fibers in the composite as a function of deformation temperature (**b**).

In the composite, the evolution of matrix was qualitatively similar to that observed in the alloy (Figure 3d–f). However, a considerably higher globularization rate was noted (Figure 4a) due to which much more homogeneous microstructures were formed after hot deformation. Furthermore, the fraction of the globularized structure increased with temperature from ~40 to ~80% in the alloy and from ~55 to ~90% in the composite. The size of α-particles in the alloy and composite did not differ noticeably; for example, after compression at 950 °C, the size of α-particles was 2.5 $\pm$ 0.5 μm and 3.2 $\pm$ 0.5 μm in the alloy and composite, respectively. The volume fraction of the β-phase increased with increasing deformation temperature from 2 vol.% (at T = 800 °C) to 30 vol.% (at T = 950 °C) in the alloy and from 1 vol.% (at T = 800 °C) to 15 vol.% (at T = 950 °C) in the composite.

The TiB fibers also rotated towards the metal flow direction during hot deformation (Figure 3d–f). In addition, considerable shortening of the TiB fibers from 25 μm in the initial condition to 5–7 μm after hot compression was noted (Figure 4b). The average diameter of TiB fibers slightly decreased after high-temperature deformation to ~0.8 μm in the temperature range of 800–950 °C in comparison with the initial value of ~2.6 μm. Thus, after deformation, the value of the length-to-diameter ratio was found to be $\leq$10 due to which the Orowan strengthening mechanism can be considered as the main strengthening mechanism for the composite [17].

The results of TEM analysis also suggest a faster globularization development in the composite in comparison with the unreinforced alloy (Figure 5). Even after compression at 950 °C, some parts of the microstructure preserved the lamellar morphology of the phases, and the onset of dynamic recrystallization was only observed in the α-phase (Figure 5a). However, in more favorably oriented colonies, the development of recrystallization/globularization can result in the formation of a globular microstructure (Figure 5b).

In the Ti-6.5Al-2Zr-1Mo-1V/TiB composite, the globular microstructure was mainly observed after compression at 800 °C (Figure 6a). The microstructure consisted of equiaxial particles of the α- and β-phases with a moderate or low dislocation density (Figure 6a). Higher deformation temperature did not result in a pronounced difference in the characteristics of the microstructure at the micro-level, although some microstructure coarsening and almost complete globularization can be noticed after deformation at 950 °C (Figures 3f and 6b).
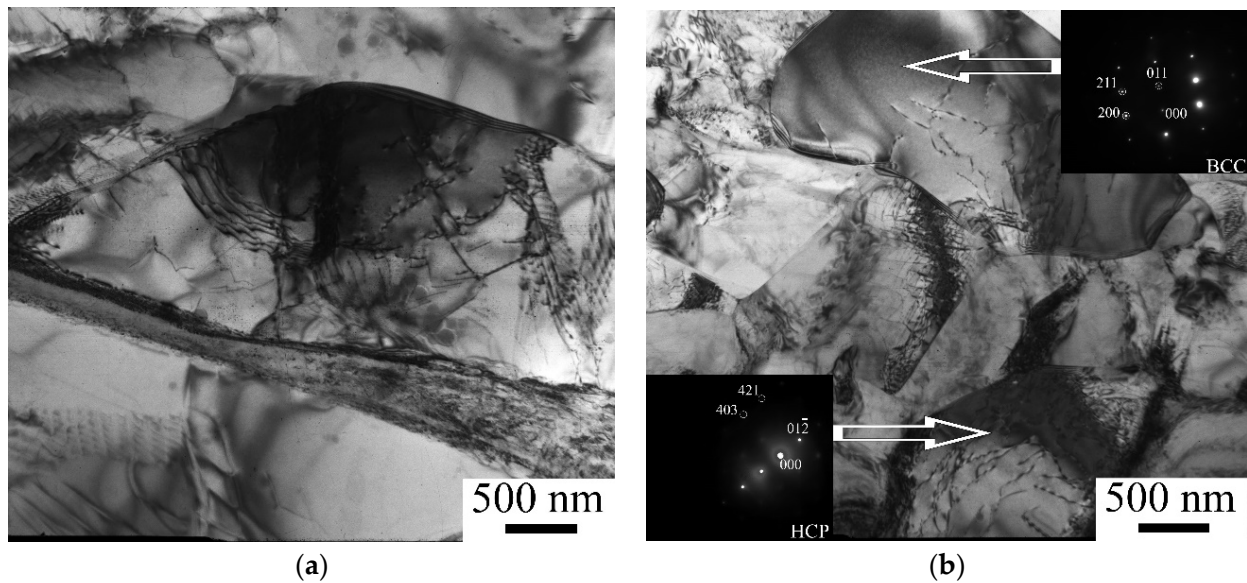
Figure 5. TEM images of the Ti-6.5Al-2Zr-1Mo-1V unreinforced alloy compressed at 950 °C; lamellar structure and globular α-particle (**a**), a globular microstructure (**b**).
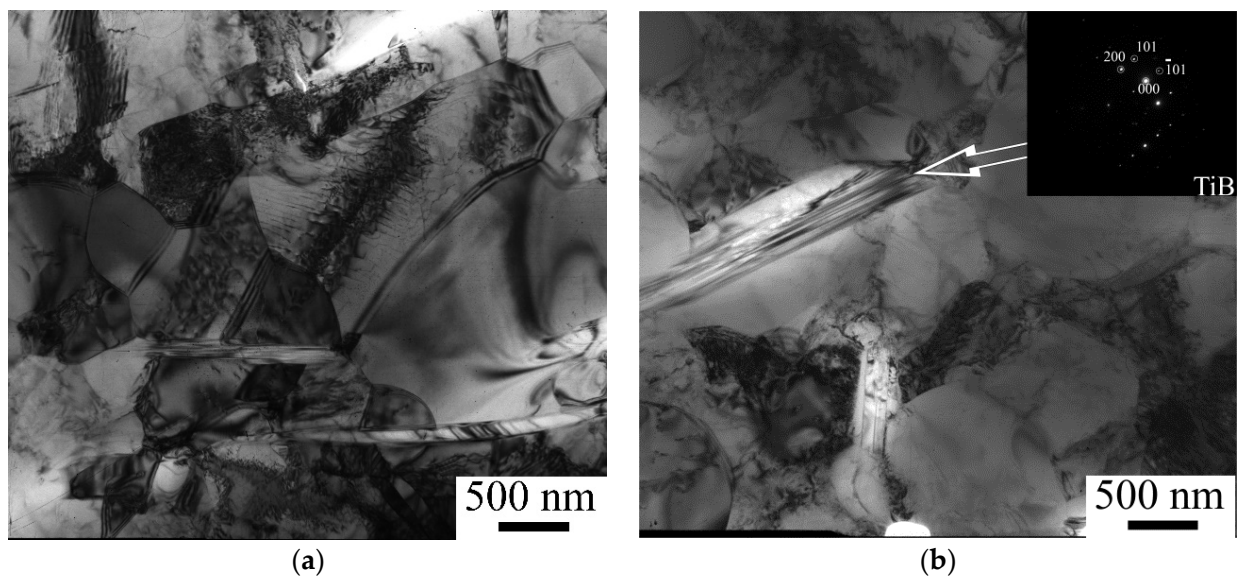

Figure 6. TEM images of the Ti-6.5Al-2Zr-1Mo-1V/TiB composite compressed at 800 °C (**a**) or at 950 °C (**b**).

In the areas located near the TiB particles, the microstructure also evolved via the re-crystallization and globularization processes; in some cases, the interphase particle/matrix interface served as a substrate for a new grain formation (Figure 6b). At the same time, the interphase particle/matrix boundary did not contain either a transition layer or any defects like pores or microcracks.

4. Discussion

The obtained results demonstrated several effects of borides on the structure evolution and high-temperature mechanical properties of the Ti-6.5Al-2Zr-1Mo-1V alloy. The most intriguing of them is associated with an increase in the high-temperature strength of the composite in comparison with that of the alloy. Indeed, our results show that, during short time tests (conventional compression), the strength characteristics of the composite was ~ 2 times higher in comparison with those of the alloy (Table 1, Figure 2). Furthermore,

it should be noted that a higher creep resistance has been reported earlier for other TiB-reinforced Ti alloys [5,6,19]; however, these data were obtained for composites with a so-called network structure in which TiB was regularly distributed around particles of the alloy powder. It should also be noted that no catastrophic drop in ductility was observed in the composite in comparison with the unreinforced alloy.

One of the most obvious effects is associated with a noticeably faster globularization of the composite in comparison with the unreinforced alloy (Figures 3 and 4a). The coarse TiB fibers are distributed in the composite quite randomly, but they form micro-volumes that are free of borides. The size of these micro-volumes is associated with the average spacing between fibers (i.e., ~26 μm). Deformation within each micro-volume is constrained by the surrounding fibers due to which the microstructure evolution in the micro-volume develops more-or-less independently and thus more homogeneously. In fact, a similar effect was observed in Ti-6Al-4V alloy, in which the microstructure evolution within each phase (α and β) intensified with the transition of the α/β interphase boundary from a semi-coherent to a non-coherent state. Moreover, the microstructure refinement (considering the average effective size during globularization as the spaces between fibers) can also contribute to some increase in deformation homogeneity. In this case, the orientation of the α-colonies with respect to the compression direction may not be that important for the composite, while in the alloy, these colonies, in which α-colonies are oriented along the plastic flow direction, demonstrate the lowest globularization rate [20].

This "constrained" plastic strain and a more homogeneous deformation within each micro-volume in the composite in comparison with the alloy can result in quite an atypical processing map (Figure 7). In the case of Ti-6.5Al-2Zr-1Mo-1V alloy, the highest power dissipation efficiency (η) was observed for the lowest strain rate (5×10^{-4} s^{-1}) and the highest temperature (950 °C) (Figure 7a), which is specific for a particular alloy [16]. In contrast, the interval of η variation in the composite is noticeably narrower (Figure 7b), suggesting a much lower sensitivity of the material both to strain rate and temperature (within the studied limits). However, the volume fraction of the globularized structure was higher in the composite; lower values of m are associated with larger α-particles obtained after deformation of the composite. Higher values of power dissipation efficiency (η) may be associated with a larger volume fraction of the β-phase in the alloy, which in turn effectively inhibits the growth of the α-particles at high temperatures. Strain localization in the β-phase also leads to a smaller volume fraction of the globularized structure in the alloy in comparison to that of the composite. Diffusion in the β-phase in $\alpha + \beta$-phase titanium alloys is faster than that in the α-phase [21]. However, quite a wide interval of instability can be noticed at temperatures below ~850 °C. The features of the composite may be not adequate from the technological point of view since it narrows the technological window, impeding the selection of proper thermomechanical parameters; however, the insensitivity to temperature can also suggest potentially higher operating temperatures.

Evaluation of the activation energy of deformation also suggests a better performance of the composite at elevated temperatures. For temperatures between 750 and 950 °C, the experimental dots (in terms of log–log dependence of strain rate on stress) can be approximated well using a linear dependence, with the average slope n of 4.14 for the alloy (Figure 8a) and of 5.19 for the composite (Figure 9a), respectively. The Arrhenius semi-log plots of steady-state flow stress vs. inverse temperature at four strain rates for both the alloy and composite are shown in Figures 8b and 9b. The calculated values of activation energy of deformation Q were found to be 388 kJ/mol for the alloy and 413 kJ/mol for the composite. A higher activation energy for the composite in comparison with the alloy was reported earlier, and usually, this phenomenon was attributed to the effective inhibition of the movement of dislocations due to the presence of the borides [22].
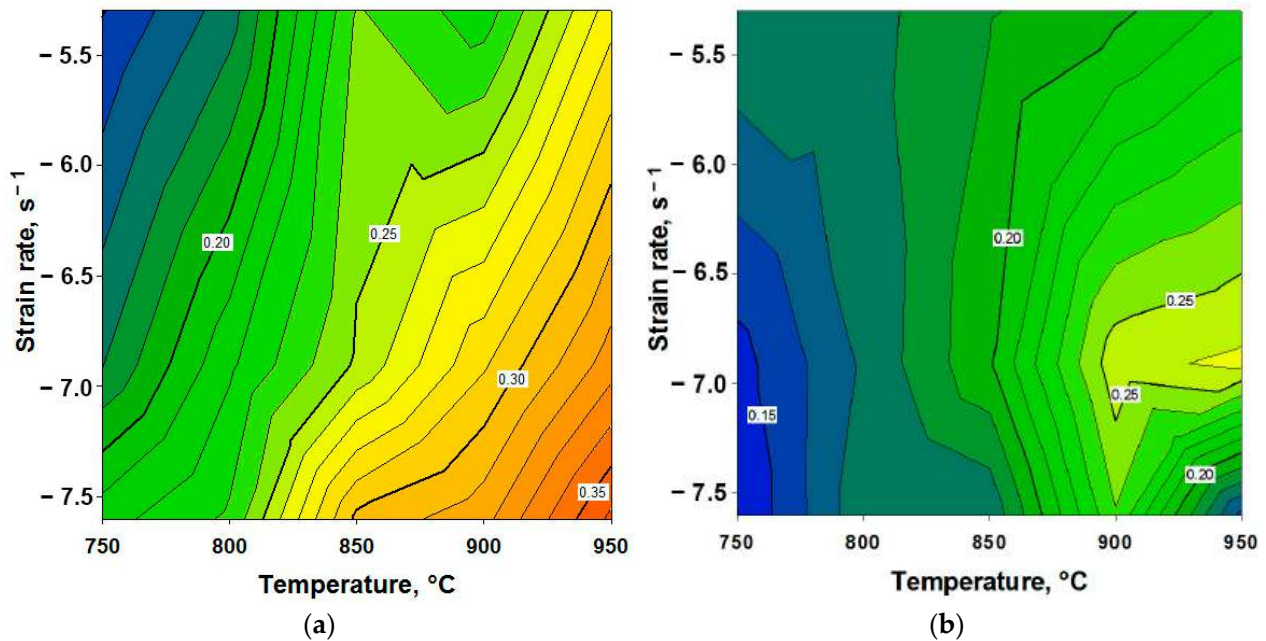
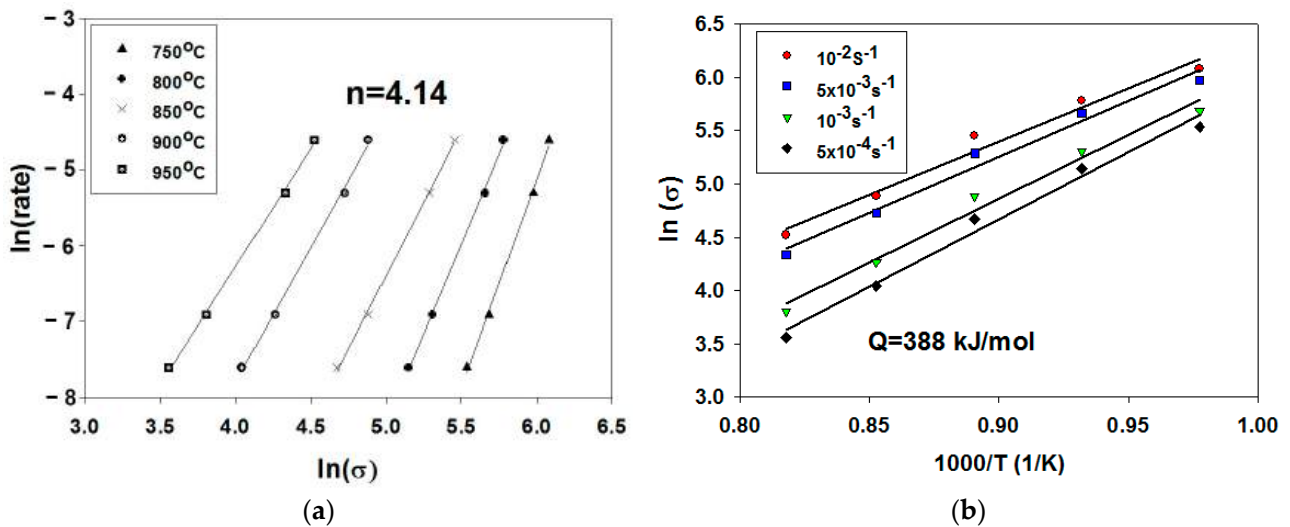**Figure 7.** Processing maps for the unreinforced alloy (**a**) and the composite (**b**).

Figure 8. Log–log dependence of strain rate on stress (**a**) and Arrhenius semi-log plot of steady-state flow stress vs. inverse temperature (**b**) for the unreinforced alloy compressed in the interval of T = 750–950 °C.

Meanwhile, the observed values of activation energy are much higher than those observed during the deformation of composites with a single-phase matrix: hcp in Ti/TiB ($n \approx 7$ and Q = 168 kJ/mol in the α phase field) [22] and bcc in Ti-15Mo/TiB ($n \approx 5$ and Q = 241 kJ/mol in the β phase field) [18]. The obtained values are also much higher than those for self-diffusion in α titanium (150 kJ/mol) [23]; however, they are quite close to the interval of Q = 250–330 kJ/mol reported for glide along the prism planes when the thermally activated overcoming of solute atoms is the main rate-controlling mechanism [24]. Some increase in the values of activation energy can also be associated with the development of dynamic recrystallization and/or globularization [25]. These assumptions correspond well with the result of microstructure analysis (Figure 3, Figure 5, and Figure 6).
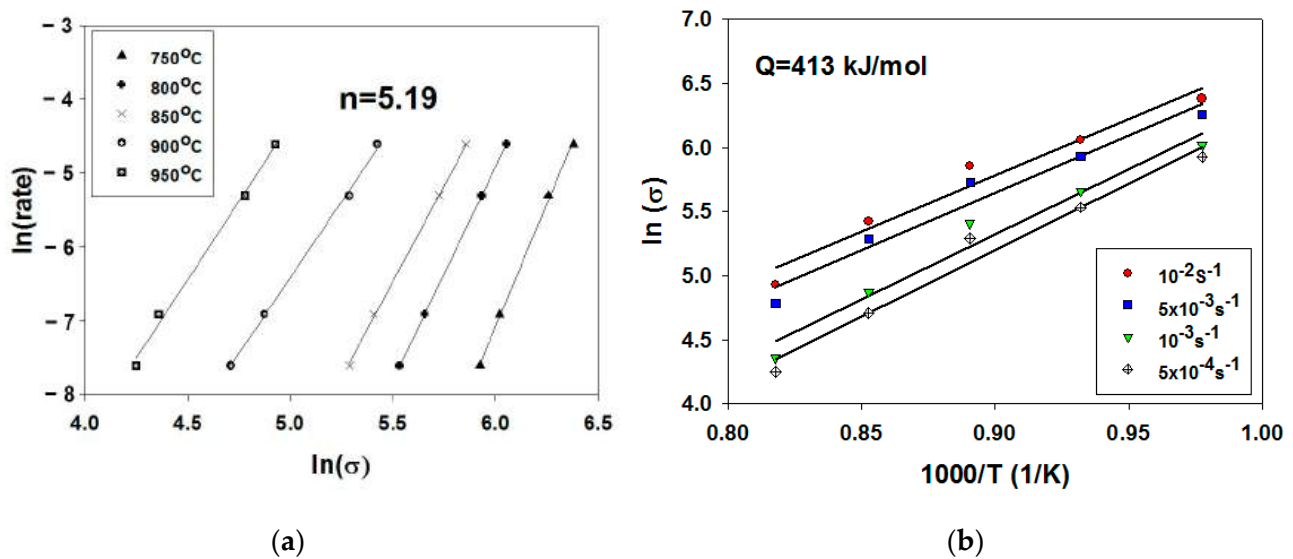
(**a**)

(**b**)

Figure 9. Log–log dependence of strain rate on stress (**a**) and Arrhenius semi-log plot of steady-state flow stress vs. inverse temperature (**b**) for the composite compressed in the interval of T = 750–950 °C.

5. Conclusions

In this work, TiB fibers were introduced into the Ti-6.5Al-2Zr-1Mo-1V alloy matrix, and the effect of fibers on the microstructure and mechanical properties of the unreinforced alloy in the interval of 20–950 °C was studied. The drawn conclusions are as follows:

(1) The initial structure of the as-cast Ti-6.5Al-2Zr-1Mo-1V alloy consisted of colonies of α-lamellae in the β-matrix. The size of α-colonies and β-grains were found to be ~100 μm and ~2 mm, respectively. The 6.5Al-2Zr-1Mo-1V/TiB composite in the initial as-cast condition comprised of the two-phase α/β matrix with a relatively homogeneous distribution of TiB fibers. The TiB fibers had a needle-like shape with a prismatic cross-section; the faces of TiB were created by the (100), (101), and (10$\bar{1}$) planes. The average apparent length and cross-section of TiB fibers were ~26 μm and ~2.6 μm, respectively. The volume fraction of TiB in the composite was found to be ~10%.

(2) The addition of 10.0 vol.% of TiB significantly influenced the mechanical properties of the composite in comparison with the unreinforced alloy. At room temperature, the yield strength of the Ti-6.5Al-2Zr-1Mo-1V alloy turned out to be equal to 800 MPa, and ductility was 18%. The TiB fibers contributed to a 40% increase in strength to a value of 1100 MPa. At 400 °C, the specimens of both states fractured in the deformation range of ~10–15%, and the yield strength values were 470 MPa for the unreinforced alloy and 750 MPa for the composite. The yield strength of the composite remained ~1.5–2 times higher till 950 °C compared to the unreinforced alloy.

(3) The microstructure evolution of the alloy during its deformation at 800–950 °C is associated with either alignment of α-lamellae along the metal flow direction or globular-ization of the α-phase, depending on the initial spatial orientation. A faster development of globularization in the composite compared to the unreinforced alloy was observed. The interphase TiB particle/matrix boundary did not contain either a transition layer or any defects like pores or microcracks.

(4) The calculated activation energy of plastic deformation Q was found to be 388 kJ/mol for the unreinforced alloy and 413 kJ/mol for the composite.

References

1. Williams, J.C.; Boyer, R.R. Opportunities and Issues in the Application of Titanium Alloys for Aerospace Components. *Metals* **2020**, *10*, 705. [CrossRef]
2. Pushp, P.; Dasharath, S.M.; Arati, C. Classification and applications of titanium and its alloys. *Mater. Today* **2022**, *54*, 537–542. [CrossRef]
3. Sun, Q.J.; Xie, X. Microstructure and mechanical properties of TA15 alloy after thermo-mechanical processing. *Mater. Sci. Eng. A* **2004**, *724*, 493–501. [CrossRef]
4. Sun, Z.; Yang, H. Microstructure and mechanical properties of TA15 titanium alloy under multi-step local loading forming. *Mater. Sci. Eng. A* **2009**, *523*, 184–192. [CrossRef]
5. Hayat, M.D.; Singh, H.; He, Z.; Cao, P. Titanium metal matrix composites: An overview. *Compos. Part A Appl. Sci. Manuf.* **2019**, *121*, 418–438. [CrossRef]
6. Shetty, R.; Hegde, A.; Shetty SV, U.K.; Nayak, R.; Naik, N.; Nayak, M. Processing and Mechanical Characterisation of Titanium Metal Matrix Composites: A Literature Review. *J. Compos. Sci.* **2022**, *6*, 388. [CrossRef]
7. Morsi, K. Review: Titanium–titanium boride composites. *J. Mater. Sci.* **2019**, *54*, 6753–6771. [CrossRef]
8. Lin, J.; Stinnett, T.C. Development of thermal barrier coatings using reactive pulsed dc magnetron sputtering for thermal protection of titanium alloys. *Surf. Coat. Technol.* **2020**, *403*, 126377. [CrossRef]
9. Fröhlich, M.; Braun, R.; Leyens, C. Oxidation resistant coatings in combination with thermal barrier coatings on γ-TiAl alloys for high temperature applications. *Surf. Coat. Technol.* **2006**, *201*, 3911–3917. [CrossRef]
10. Zhang, C.J.; Kong, F.T.; Xu, L.J.; Zhao, E.T.; Xiao, S.L.; Chen, Y.Y.; Deng, N.J.; Ge, W.; Xu, G.J. Temperature dependence of tensile properties and fracture behavior of as rolled TiB/Ti composite sheet. *Mater. Sci. Eng. A* **2012**, *556*, 962–969. [CrossRef]
11. Imayev, V.M.; Gaisin, R.A.; Imayev, R.M. Microstructure and mechanical properties of near a titanium alloy based composites prepared in situ by casting and subjected to multiple hot forging. *J. Alloys Compd.* **2018**, *762*, 555–564. [CrossRef]
12. Ozerov, M.; Klimova, M.; Sokolovsky, V.; Stepanov, N.; Popov, A.; Boldin, M.; Zherebtsov, S. Evolution of microstructure and mechanical properties of Ti/TiB metal-matrix composite during isothermal multiaxial forging. *J. Alloys Compd.* **2019**, *770*, 840–848. [CrossRef]
13. Yang, J.H.; Xiao, S.L.; Chen, Y.Y.; Xu, L.J.; Wang, X.P.; Tian, J.; Zhang, D.D.; Zheng, Z.Z. Microstructure evolution during forging deformation of (TiB+TiC+Y2O3)/α-Ti composite: DRX and globularization behavior. *J. Alloys Compd.* **2020**, *827*, 154170. [CrossRef]
14. Qiu, P.; Le, J.; Han, Y.; Chen, Y.; Huang, G.; Mao, J.; Lei, L.; Lu, W. Superior superplasticity and multiple accommodation mechanisms in TiB reinforced near-α titanium matrix composites. *Compos. Part B Eng.* **2022**, *238*, 109940. [CrossRef]
15. Jia, L.; Li, X.; Kondoh, K.; Chen, B.; Li, S.F.; Umeda, J.; Lu, Z.L. Hybrid effect of TiCp and TiBw co-strengthening Ti matrix composites prepared by spark plasma sintering and hot extrusion. *Mater. Charact.* **2019**, *151*, 6–14. [CrossRef]
16. Prasad, Y.V.R.K.; Rao, K.P.; Sasidhara, S. *Hot Working Guide: A Compendium of Processing Maps*; ASM International: Novelty, OH, USA, 2015; pp. 1–625.
17. Chen, B.; Shen, J.; Ye, X.; Jia, L.; Li, S.; Umeda, J.; Takahashi, M.; Kondoh, K. Length effect of carbon nanotubes on the strengthening mechanisms in metal matrix composites. *Acta Mater.* **2017**, *140*, 317–325. [CrossRef]
18. Zherebtsov, S.; Ozerov, M.; Klimova, M.; Moskovskikh, D.; Stepanov, N.; Salishchev, G. Mechanical behavior and microstructure evolution of a Ti-15Mo/TiB titanium–matrix composite during hot deformation. *Metals* **2019**, *9*, 1175. [CrossRef]
19. Zheng, Y.; Xu, L.; Chi, D.; Liang, Z.; Han, S.; Xue, X.; Xiao, S.; Tian, J.; Chen, Y. Tensile and creep properties under different temperature conditions of titanium matrix composites reinforced by TiB and TiC. *Mater. Sci. Eng. A* **2022**, *860*, 144279. [CrossRef]
20. Jiang, Y.Q.; Lin, Y.C.; Zhao, C.Y.; Chen, M.S.; He, D.G. A New Method to Increase the Spheroidization Rate of Lamellar α Microstructure during Hot Deformation of a Ti–6Al–4V Alloy. *Adv. Eng. Mater.* **2020**, *22*, 2000447. [CrossRef]
21. Mishin, Y.; Herzig, C. Diffusion in the Ti–Al system. *Acta Mater.* **2000**, *48*, 589–623. [CrossRef]

22. Ozerov, M.; Klimova, M.; Kolesnikov, A.; Stepanov, N.; Zherebtsov, S. Deformation behavior and microstructure evolution of a Ti/TiB metal-matrix composite during high-temperature compression tests. *Mater. Des.* **2016**, *112*, 17–26. [CrossRef]

23. Frost, H.J.; Ashby, M.F. *Deformation-Mechanism Maps*; Pergamon Press: Oxford, UK, 1982; pp. 1–166.

24. Conrad, H. Effect of interstitial solutes on the strength and ductility of titanium. *Prog. Mater. Sci.* **1981**, *26*, 123–403. [CrossRef]

25. Raj, S.V.; Langdon, T.G. Creep behavior of copper at intermediate temperatures—I. Mechanical characteristics. *Acta Metall.* **1989**, *37*, 843–852. [CrossRef]